Investigation of Organic Rankine Cycle Integrated with Double Latent Thermal Energy Storage for Engine Waste Heat Recovery

Xiaoli Yu [a,b], Zhi Li [a,b], Yiji Lu [a,b,*], Rui Huang [a], Anthony Paul Roskilly [a,b]

[a] *Department of Energy Engineering, Zhejiang University, Hangzhou, 310027, China*

[b] *Sir Joseph Swan Centre for Energy Research, Newcastle University, Newcastle NE1 7RU, UK*

Highlights:

- ORC integrated with double LTES for engine waste heat recovery is proposed
- Twelve inorganic-salt PCMs are screened and the optimal one has been identified
- System output performance under different LTES volume is studied
- Three different scenarios integrated with single or double LTES are compared

Abstract

In this work, organic Rankine cycle (ORC) integrated with Latent Thermal Energy Storage (LTES) system for engine waste heat recovery has been proposed and investigated to potentially overcome the intermittent and fluctuating operational conditions for vehicle applications. A melting-solidification model has been established to investigate and compare the performance of twelve Phase Change Materials (PCMs) under different heat source conditions. Among the twelve PCMs, $LiNO_3$-KCl-$NaNO_3$ is identified as the optimal PCM for engine exhaust heat recovery. The performance of the ORC system integrating with different volume of LTES using $LiNO_3$-KCl-$NaNO_3$ under dynamic heat source simulating vehicle conditions is studied. Results illustrate the fluctuation of engine exhaust heat can be potentially

* Corresponding author.

E-mail address: yiji.lu@zju.edu.cn; luyiji0620@gmail.com (Y. Lu)

overcome by using the proposed solution. The condition of 100 L LTES provides 30.4% larger total output work than that of 50 L LTES, while it is merely 1.5% larger than that of 90 L LTES. The performance of three different LTES-ORC scenarios are compared and results show ORC combining with double LTES delivers 17.2% larger total power output than that of single LTES (100 L) under the same operational conditions.

Keywords: Latent Thermal Energy Storage, Phase Change Material, Organic Rankine Cycle, Dynamic Heat Source, Engine Waste Heat Recovery

Nomenclature

A_{in}	Area of exhaust side (m^2)
A_{out}	Area of working fluid side m^2
c_i	The specific heat capacity of exhaust at time interval *i* (kJ/kg K)
c_{melt}	The specific heat capacity of exhaust at T_{melt}. (kJ/kg K)
Cp	The specific heat capacity of PCM (kJ/kg K)
Cp_c	The specific heat capacity of coolant (kJ/kg K)
Cp_{exh}	The specific heat capacity of the exhaust (kJ/kg K)
Cp_l	The specific heat capacity of liquid PCM (kJ/kg K)
Cp_s	The specific heat capacity of solid PCM (kJ/kg K)
d	The diameter of the exhaust pipe (m)
h_{exh}	Heat transfer coefficient of the exhaust ($W \cdot m^{-2}\ K^{-1}$)
h_{in}	Enthalpy of working fluid at the inlet of LTES ($kJ \cdot kg^{-1}$)

h_{out}	Enthalpy of working fluid at the outlet of LTES ($kJ \cdot kg^{-1}$)
h_{wf}	Heat transfer coefficient of working fluid ($W \cdot m^{-2}\ K^{-1}$)
$h_{wf,l}$	Heat transfer coefficient of working fluid at liquid zones ($W \cdot m^{-2}\ K^{-1}$)
$h_{wf,tp}$	Heat transfer coefficient of working fluid at two-phase zones ($W \cdot m^{-2}\ K^{-1}$)
i	n^{th} time interval
ΔL	Latent heat of PCM ($kJ \cdot kg^{-1}$)
mc	The mass flow rate of coolant (kg/s)
m_i	The mass flow of exhaust at time interval i ($kg \cdot s^{-1}$)
$m_{exh,i}$	The mass flow rate of exhaust at time interval i ($kg \cdot s^{-1}$)
m_{wf}	The mass flow rate of working fluid ($kg \cdot s^{-1}$)
m_{PCM}	Total mass of PCM (kg)
Nu_{exh}	Nusselt number of exhaust gas
Pr_{exh}	Prandtl number of exhaust gas
Q_{exh}	Heat flux the exhaust released to PCM (kW)
Q_{in}	Heat flux received from the evaporator (kW)
Q_{out}	Heat dissipation at condenser (kW)
Q_{store}	Thermal energy stored by the PCM (kJ)
$Q_{store,max}$	Maximum thermal energy stored by the PCM (kJ)
Q_{wf}	Heat the working fluid absorbed from PCM (kW)
Re_{exh}	Reynolds number of exhaust gas
T_0	The initial temperature of PCM at solid state (°C)

$T_{e,pp}$	Evaporator pinch point temperature difference
T_{evap}	Evaporating temperature (℃)
$T_{exh,in}$	The inlet temperature of the exhaust (℃)
$T_{exh,out}$	The outlet temperature of the exhaust (℃)
T_i	The temperature of exhaust at time interval i
T_{melt}	Melting temperature of PCM (℃)
T_{PCM}	The temperature of PCM (℃)
$\Delta T_{lm,char}$	Log mean temperature difference in the charging process (℃)
$\Delta T_{lm,disc}$	Log mean temperature difference in the discharging process (℃)
$T_{e,pp}$	Evaporator pinpoint temperature difference (℃)
Δt_1	Time step in the charging process (s)
Δt_2	Time step in the discharging process (s)
V	The volume of PCM (L)
W_p	Work consumed by the pump (kW)
W_e	Output work of expander (kW)
W_{net}	The net power output of ORC (kW)
Greek letters	
$\Delta\beta_{char}$	The liquid mass fraction of the charging process
$\Delta\beta_{disc}$	The liquid mass fraction of the discharging process
λ_{exh}	The thermal conductivity of exhaust
ρ_s	The density of PCM at slid state

$\Delta\tau$	Length of discretized time
η_{sE}	Expander isentropic efficiency
η_{sP}	Pump isentropic efficiency
η_{th}	The thermal efficiency of the ORC system
Acronym	
ETC	European Transient Cycle
HTF	Heat Transfer Fluid
ICE	Internal Combustion Engine
LTES	Latent Thermal Energy Storage
ORC	Organic Rankine Cycle
TLC	Trilateral Rankine cycle

1

2

1. Introduction

Increasing attention is focusing on the environmental problems caused by the emissions from burning fossil fuels [1, 2]. Integrating waste heat recovery system to the existing energy systems can be a potential solution to improve the overall system efficiency and reduce the consumption of conventional energy resources. For vehicle application, the Internal Combustion Engine (ICE) dissipates around 60-70% of the overall fuel energy through exhaust gas, engine coolant, exhaust gas recirculation and charge air cooler [3, 4]. Several Rankine based systems have been proposed by researchers to study the performance of different waste heat recovery technologies, which can be used to recover the engine waste heat [5-7]. Other solutions such as thermoelectric generator [8, 9] and chemical absorption [10, 11] to recover the engine waste heat have also been reported. Among all these proposed waste heat recovery technologies, Organic Rankine Cycle (ORC) has been considered as one of the most practical solutions because of its simplicity, reliability, flexibility and relatively high efficiency [12].

The mainstream methods to investigate ORC technologies include the investigation of different ORC working fluids [13, 14], optimisation of system parameters [15, 16], design and optimisation of components [17] such as heat exchanger and expander, and the design of system configurations. Wang et al. [13] proposed a method to select working fluids and conduct parametric optimisation using a multi-objective optimisation model based on the simulated annealing algorithm. Results indicated R123 is the best candidate under the temperature ranging from 100-180 ^{o}C [13]. When the heat source temperature is higher than 180 ^{o}C, R141b is the optimal working fluid for the ORC system [13]. The investigation of the

ORC system using alkane working fluids due to their excellent thermo-physical and environmental characteristics for engine waste recovery was reported by Shu et al [14]. Six indicators including thermal efficiency, exergy destruction factor, turbine size parameter, total exergy destruction rate, turbine volume flow ratio and net power output per unit mass flow rate of exhaust were adopted to study the performance of the ORC system using Alkane-based working fluids [14]. Yang et al. [15] developed a thermo-economic model to study a dual-loop organic Rankine cycle and employed a multi-objective genetic algorithm to obtain the Pareto optimal solutions. The maximum net power output and the minimum total economic cost during the whole range of operating conditions for a CNG engine were investigated [15]. Liu et al. [16] established a heat transfer model for a fin-and-tube evaporator of the ORC system to recover the waste heat of a diesel engine. Particle swarm optimisation algorithm is adopted to study the key geometric parameters of the fin-and-tube evaporator including the inlet radius of tube side and a shell side, height and thickness of fins and fin spacing. Ayad M. et al. [17] used small-scale axial, radial-inflow and radial outflow turbines on a small scale ORC system and compared their performances under their single and two stage configurations based on three-dimensional CFD analysis. Results indicated the two-stage axial and radial-outflow configurations can achieve a considerably better performance [17].

Many researchers are approaching to design and study cascaded ORC technologies to fully recover the engine waste heat. For example, Song et al. [18, 19] investigated a cascade ORC system designed for a heavy-duty diesel engine. Results showed R236fa was the most suitable selection for LT loop while cyclohexane and water were the proper working fluids for the HT

loop. The system can potentially improve the engine power by 11.2-11.6%. Yari et al. [20] compared the performance of organic Rankine cycle, trilateral Rankine cycle and Kalina cycle for recovering low-grade waste heat considering based on the thermodynamic and thermo-economic analysis. The results revealed that the Trilateral Rankine cycle (TLC) can obtain a larger net output power than that of the ORC and Kalina systems. Yu et al. [21] proposed an innovative cascade cycle combining a Trilateral Cycle and an ORC for industry or transport application to recover the exhaust thermal energy. Compared to the performance of a conventional dual-loop ORC system, the proposed novel cycle can improve the overall thermal efficiency and exergy efficiency by 33.7% and 31.2%, respectively [21].

For vehicle application due to the instantaneously operating conditions of the engines, the investigation of the dynamic performance of ORC systems attracted increasing attention. However, most of the studies focused on the performance of ORC under steady operating conditions of vehicle engines without considering the randomly and frequently operating conditions in the practical application. The violent fluctuation of engine exhaust mass flow rate and temperature lead to the unsteady ORC system operational state, which could damage the ORC system. When the inlet temperature at turbine inlet is out of the designed conditions, the ORC system works in a low efficient mode [22]. On the other hand, when the exhaust heat cannot provide sufficient heat to maintain the ORC systems operating within the designed conditions, the unsaturated working fluid will damage the expansion machine due to the existence of droplet [23]. The performance parameters of ORC systems such as thermal efficiency and net power output change greatly under different engine operating loads. Shu et

al. [24] studied the influence of engine operating conditions on a cascaded ORC system. When the temperature and mass flow rate of exhaust gas varies from 326 ℃ at 457.07 kg/h to 519 ℃ at 990.79 kg/h, the net power output and thermal efficiency change from about 12 kW at 6% to 38 kW at 12% [24]. Katsanos et al. [25] investigated the potential improvement in the overall efficiency of a heavy-duty truck diesel engine equipped with an ORC system recovering engine exhaust heat. Results shown that the specific fuel consumption improvement ranging from 10.2% (at 25% engine load) to 8.5% (at 100% engine load). In order to overcome the frequency variation of engine conditions, the ORC system with an oil storage was adopted and experimentally investigated by Shu et al. [23]. The results indicated that thermal oil loop brought a significant inertia to the response of a system which could be positive against the variation of engine condition. However, large space will be required to place the oil loop and related auxiliary devices, which is less possible to meet the requirement of compactness for the vehicle applications. Compared to the sensible heat storage method, latent thermal energy storage using Phase Change Material (PCM) possesses larger energy storage density with smaller volumes [26], and it can also provide a relatively homogeneous temperature field due to the phase change process of PCM. Therefore, LTES has the potential to be used for waste heat recovery and is suitable to bridge the mismatch between the energy supply and demand [27]. The energy storage device can act as a flywheel storing the waste heat of exhaust gas when the engine works under high load and releasing the stored heat to the ORC system when the engine works under low load.

Integrating PCM latent thermal energy storage systems for recovering waste heat of engine

exhaust gas can be a potential solution. However, very limited researches have been found in the literature due to the concerns of system complicity and cost. Magro et al. [28] designed a PCM-based ORC recovering heat system for a billet reheating furnace. The conclusion is that the PCM-based technology can effectively reduce the adverse effects of fluctuating industrial waste heat and increase the average thermal efficiency from 15.5% to 16.4% and guarantee a payback period between 3 and 5 years [28]. Magro et al. [29] reported a study of a PCM-coupled steam generator for steel waste heat recovery. In the proposed system the thermal power fluctuation of exhaust gas was levelled in the PCM section before entering the steam generation section to generate constant superheated steam at the inlet of the turbine nearly at nominal load. The resulted showed that compared to traditional solutions the size of the steam generator and the turbine can be reduced to about 41% and the electric power can be improved by 22%. Freeman et al. [30] studied a small scale solar ORC system with various thermal energy storage media due to the fluctuation of solar irradiance intensity. A lumped model for the LTES was adopted to provide a simplified comparison of the various media. Results showed that the heat storage device with the volume of 400 L hydrated-salt PCM would increase the capital cost by 30%, but the overall cost is significantly lower than equivalent electricity storage solution [30]. The performance advantages achieved by PCM are mainly determined by the selection of suitable product with suitable melting temperature [30]. Manfrida et al. [31] investigated the operation of a solar power plant associated with an LTES and an ORC unit is simulated under dynamic (time-varying) solar radiation conditions to design a system providing constant HTF power entering the evaporator of the ORC unit.

Results showed that the system is able to provide power in 78.5% of the time over the one-week period, with weekly averaged efficiencies of 13.4% for the ORC unit [31]. Although there are some references about ORC integrated with TES for solar energy utilisation and industrial applications considering the fluctuation of solar radiation intensity and industrial waste heat recovery, the majority of the ORC systems with LTES are indirect type. The ORC working fluid cannot extract heat from the PCM directly, which means a thermal fluid loop using heat transfer fluid should be added to the whole system. In this way, the system volume can increase to a large extent, which is less potential for vehicle application. Furthermore, the knowledge about phase change material options and scenario design of PCM-based ORC system for vehicle waste heat recovery require extensive research explorations. Because the temperature and mass flow rate change more frequently than that of solar radiation intensity and the requirement of compactness for vehicle using is much stricter than that of solar ORC system.

In this paper, an ORC system integrated with latent thermal energy storage has been proposed. The main aim of this paper is to evaluate the PCM options to reduce the adverse effect of the fluctuated exhaust on the ORC performance and maintain ORC working under the designed conditions. The concept of using double latent thermal energy storages have been proposed and studied in order to overcome the various operational conditions and randomly running time for vehicle application. The proposed ORC with double LTES can effectively reduce the adverse effect of unsteady and intermittent of vehicle operating loads maintaining ORC system work under relatively steady and efficient state.

2. System description

2.1 Overall system description

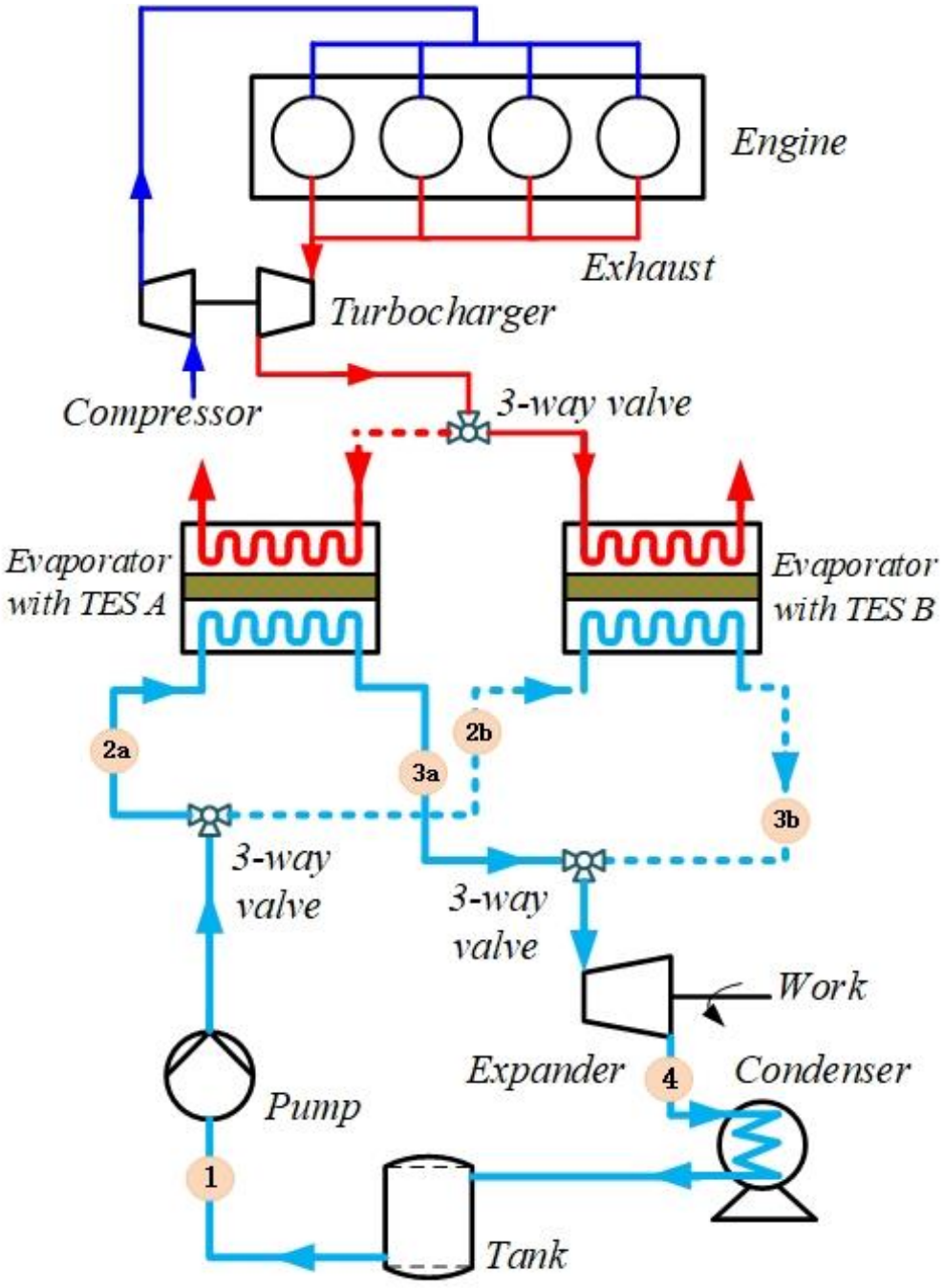

Fig. 1. Schematic diagram of the ORC integrated with double latent thermal energy storage

Fig. 1 presents the conceptual scheme of the ORC system integrated with double LTES. It

consists of two LTES evaporator, an expander, a condenser, a pump, a working fluid tank and several three-way valves. By switching three-way valves, it can be easily converted as a single LTES system.

The working process of this system can be described as follows. The high-temperature exhaust gas first flows into the LTES evaporator A, in which PCM starts the charging process and the waste heat is stored. When the PCM in the LTES evaporator A is fully melted, the exhaust gas flows into LTES evaporator B by switching the three-way valve and LTES evaporator B starts the same process as the LTES evaporator A. Meanwhile, the organic working fluid flows into LTES evaporator A and ORC starts working until the temperature of PCM decreases to the minimum driving temperature for ORC system. In this study, R245fa is adopted as the ORC working fluid, which has been previously studied for use in the low-temperature ORC waste heat recovery system and has a critical temperature of 154 ℃ [32]. The *T*-*s* diagram of ORC with LTES is illustrated in Fig. 2.

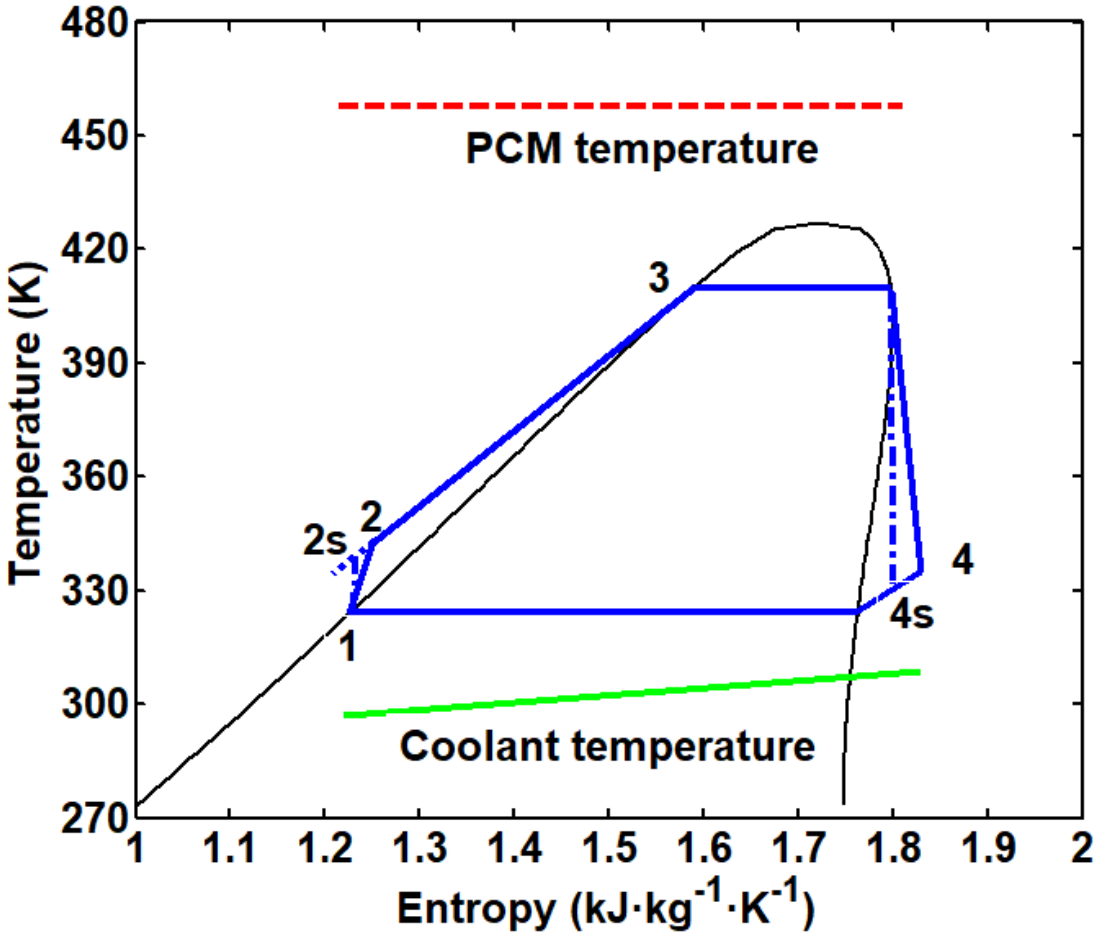

Fig. 2. *T-s* diagram of the ORC system with thermal energy storage

Evaporator with latent thermal energy storage is crucial for the performance of the whole system, in which an interlayer between the exhaust tunnel and working fluid tunnel and PCM is proposed as shown in Fig. 3. The latent thermal energy storage evaporator has a cylindrical structure including an inner tunnel, PCM interlayer and outer tunnel. The exhaust gas passes through the central channel and it heats the PCM. Fig. 4 shows the detailed structure of evaporator with LTES from the view of the longitudinal section. The shape of the PCM unit for flowing fluid heating in pipes is cylindrical geometry, which maximises the contact area with the heating target, and the structure can take high-pressure fluid.

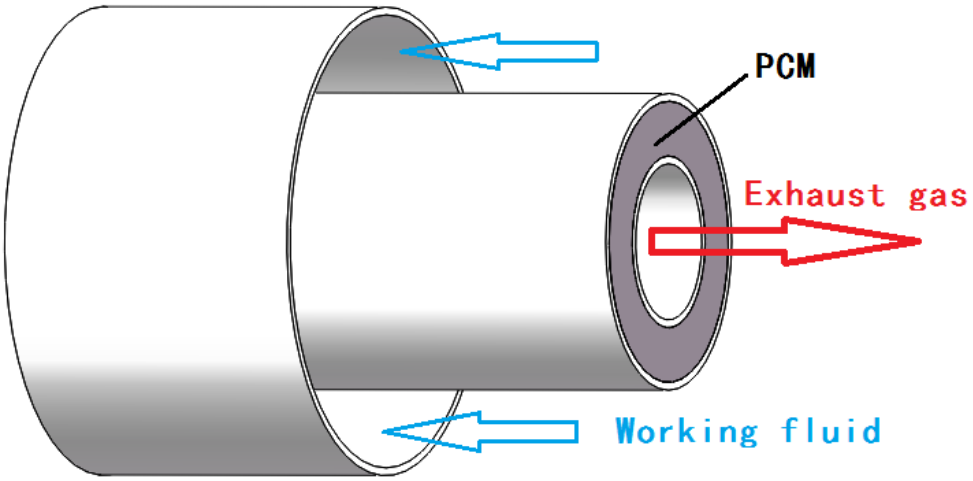

Fig. 3. Principle diagram of latent thermal energy storage evaporator

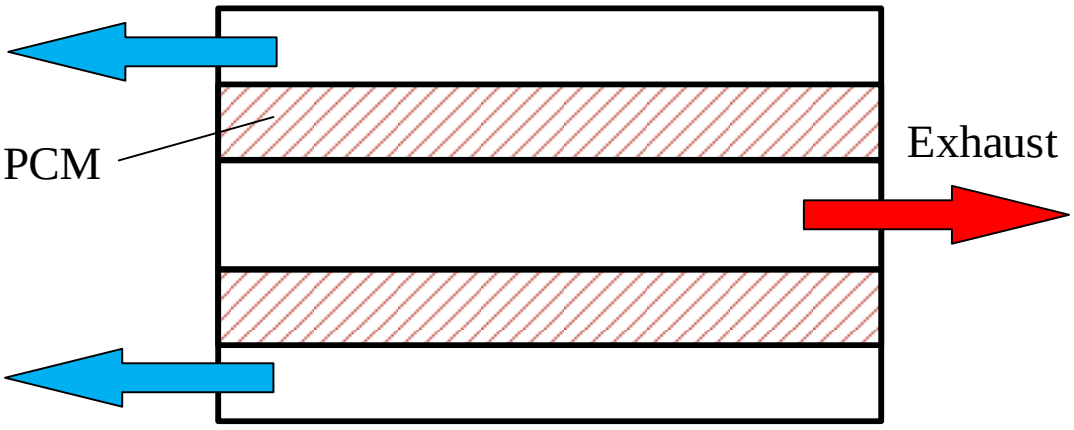

Fig. 4. Diagram of the longitudinal section of the evaporator with LTES

2.2 Phase change materials

The requirements of the ideal PCM for thermal energy storage have been listed as follows: proper melting and solidification temperature, high latent heat, the high specific heat of liquid state, high density, relatively high thermal conductivity, low vapour pressure. The average temperature of the vehicle engine exhaust gases at the inlet of ORC is around 200 to 300 ℃, therefore, the selected PCMs should have a relatively high melting temperature. In this research, inorganic eutectic-compound phase change materials are selected because they have

been widely studied for thermal storage applications. Due to their higher density and stability in their liquid state, they have been used widely as ionic liquids in high temperature sensible thermal storage systems (thermonuclear energy, concentrated solar thermal power) [33]. The physical properties chosen for the PCMs are broadly representative of a range of inorganic (hydrated-salt based) materials. Table 1 presents the detailed thermos-physical parameters of the eutectic-compound phase change materials to be studied.

Table 1. Thermo-physical properties of selected eutectic-compound phase change materials [33]

No	Eutectic compounds	Mass ratio	T_{melt}	ΔL	Cp_s	Cp_l	ρ_s
			℃	*kJ/kg*	*J/kg K*	*J/kg K*	*kg/m^3*
1	KNO_2-$NaNO_3$	48-52	149	124	1050	1630	2080
2	$LiNO_3$-$NaNO_2$	62-38	156	233	1570	1910	2296
3	$LiNO_3$-KCl	58-42	160	272	1260	1350	2196
4	$LiNO_3$-KCl-$NaNO_3$	45-5-50	160	266	1320	1690	2297
5	HCOONa-HCOOK	45-55	176	175	1150	930	1913
6	LiOH-$LiNO_3$	19-81	183	352	1600	2000	2124
7	$NaNO_3$-$LiNO_3$	51-49	194	262	1350	1720	2317
8	$NaNO_3$-KNO_3	55-45	222	110	1010	1490	2028
9	LiOH-$NaNO_3$-NaOH	6-67-27	230	184	1300	2000	2154
10	$CaCl_2$-$LiNO_3$	13-87	238	317	1500	1530	2362
11	LiCl-$LiNO_3$	9-91	244	342	1580	1610	2351

12	$NaNO_3$-NaOH	86-14	250	160	1190	1860	2241

3. Mathematical model

3.1 Design of thermal energy storage evaporator

The design criteria of LTES are determined by the latent heat of the selected PCM and waste heat of the exhaust at temperatures higher than PCM melting point T_{melt}. The maximum thermal energy stored by the PCM can be calculated as Eq. (1) [34]. $\Delta\tau$ is the length of discrete time equal to the sampling interval of the temperature data at the inlet of LTES. For each time interval i, the exhaust gas temperature T_i and the mass flow $m_{exh,i}$ are derived from the measured data shown in Fig. 5 [35], while the exhaust gas specific heat c_i is calculated as a function of T_i, as well c_{melt} is specific heat capacity of exhaust at T_{melt}.

$$Q_{stored,max} = \sum_{i:T_i>T_{melt}} \Delta\tau \cdot m_{exh,i}\left[c_i T_i - c_{melt} T_{melt}\right] \quad (1)$$

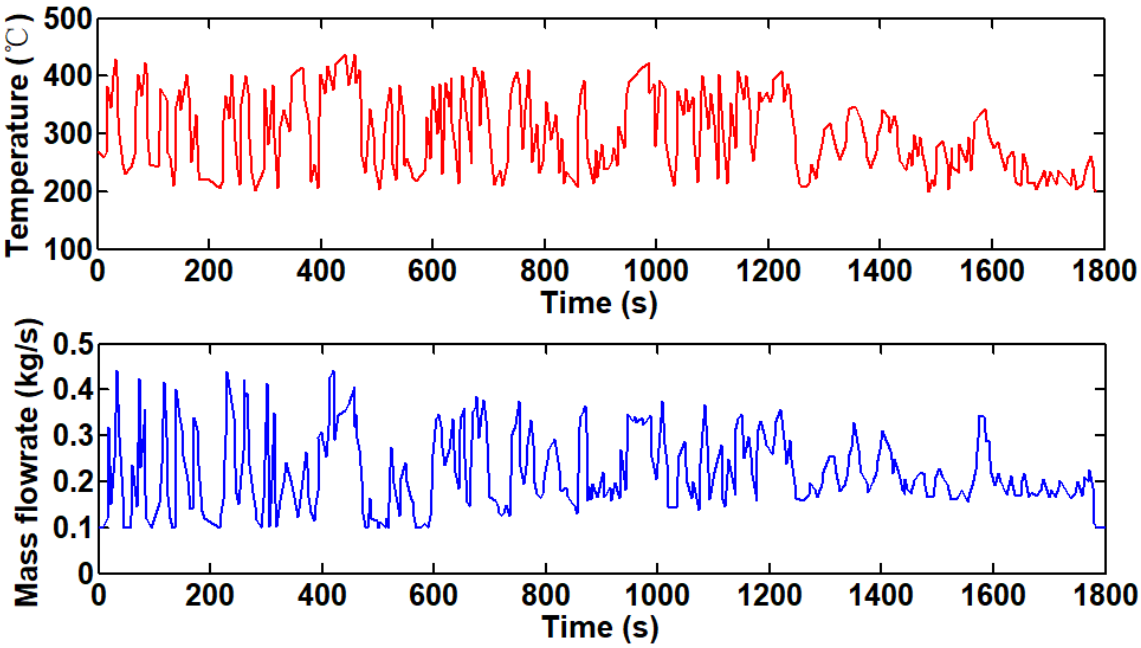

Fig. 5. Temperature and mass flow rate profiles of exhaust gas in ETC cycle [35]

Fig. 5 shows the temperature and mass flow rate profiles of vehicle diesel engine in the

European Transient Cycle (ETC). The temperature ranges from about 200 ℃ to 450 ℃ while the mass flow rate is ranging from 0.1 to 0.4 kg/s. Based on this dynamic heat source, the performance of ORC with LTES is simulated and analysed in the following sections.

PCM can store sensible heat and latent heat in the charging process. The relationship between stored heat and mass of PCM is described by

$$Q_{stored} = Cp_s m_{PCM}(T_{melt} - T_0) + \rho_s \cdot V \cdot \Delta L + Cp_l m_{PCM}(T_{PCM} - T_{melt}) \quad (2)$$

3.2 Charging process for LTES

During the charging process, the temperature of PCM rises in solid phase until it reaches up to the melting point of PCM. The temperature remains constant during the melting process. After the phase change process is completed and all the PCM turns into the liquid phase, the temperature of the liquid PCM continues to rise. The heat transfer coefficient between exhaust and PCM is calculated by Dittus-Boelter correlation [28]

$$Nu_{exh} = 0.023 Re_{exh}^{0.8} Pr_{exh}^{0.4} \quad (3)$$

$$h_{exh} = \frac{Nu_{exh} \cdot \lambda_{exh}}{d} \quad (4)$$

The log mean temperature difference $\Delta T_{lm,\,char}$ and the heat flow Q_{exh} are calculated as

$$\Delta T_{lm,char} = \frac{\left(T_{exh,in} - T_{PCM}\right) - \left(T_{exh,out} - T_{PCM}\right)}{\ln \frac{T_{exh,in} - T_{PCM}}{T_{exh,\mathrm{out}} - T_{PCM}}} \quad (5)$$

$$Q_{exh} = h_{exh} \cdot A_{in} \cdot \Delta T_{lm,char} \quad (6)$$

The heat balance reported in the following equation is used to calculate the outlet temperature

$T_{exh,\,out}$

$$Q_{exh} = m_{exh} \cdot Cp_{exh} \cdot \left(T_{exh,in} - T_{exh,out}\right) \tag{7}$$

When the calculation is converged, the relationship between the liquid mass fraction of PCM and the charging heat flow can be expressed as

$$Q_{exh} \cdot \Delta t_1 = \Delta L \cdot m_{PCM} \cdot \Delta \beta_{char} \tag{8}$$

When PCM is in the phase change process, the temperature of PCM is assumed to be constant. When PCM is in the sensible heat storage process, the updated temperature of PCM is calculated by Eq. (9), where *Cp* represents the specific heat capacity of PCM in the solid or liquid phase, which depends on its real-time state in the charging process.

$$T_{PCM}(t+1) = T_{PCM}(t) + \frac{Q_{exh}}{Cp \cdot m_{PCM}} \tag{9}$$

3.3 Discharging process for LTES

During the discharging process, thermal energy stored by liquid PCM is transferred to the heat transfer fluid (HTF). In the discharging process, the PCMs are considered as the heat source and it is assumed that one LTES is in the complete liquid state at the melting temperature while the other LTES is in the completely solid state at the melting temperature. Thermal losses in the charging and discharging process are neglected. Overall heat transfer coefficient of working fluid in liquid zones and two-phase zones are assumed to be constant [36].

The log mean temperature $\Delta T_{lm,\,disc}$ is calculated as

$$\Delta T_{lm,disc} = \frac{\left(T_{wf,in} - T_{PCM}\right) - \left(T_{wf,out} - T_{PCM}\right)}{\ln \frac{T_{wf,in} - T_{PCM}}{T_{wf,out} - T_{PCM}}} \quad (10)$$

The heat flux between PCM and the working fluid can be calculated by

$$Q_{wf} = h_{wf} \cdot A_{out} \cdot \Delta T_{lm,disc} \quad (11)$$

where h_{wf} represents the Overall heat transfer coefficient of working fluid at liquid zones and two-phase zone.

According to energy conservation, the mass flow rate of working fluid can be described as

$$m_{wf} = \frac{Q_{wf}}{(h_{out} - h_{in})} \quad (12)$$

The relationship between the liquid mass fraction of PCM and the discharging heat flow can be expressed as

$$Q_{wf} \cdot \Delta t_2 = \Delta L \cdot m_{PCM} \cdot \Delta \beta_{disc} \quad (13)$$

In the discharging process, the temperature of PCM is assumed to be constant when the PCM is during its phase change process. When PCM releases its sensible heat in the liquid or solid state, the temperature of PCM is calculated by

$$T_{PCM}(t+1) = T_{PCM}(t) - \frac{Q_{exh}}{Cp \cdot m_{PCM}} \quad (14)$$

3.4 Thermodynamic model for ORC

The temperature of PCM is assumed to be constant when it releases stored heat to the working fluid during the discharging process (solidification process). The key parameters for the sizing

of the ORC system in conjunction with the LTES are the working fluid mass flow rate and the evaporation temperature. The evaporating temperature should meet the requirements of liquid-liquid heat exchangers and gas-liquid heat exchangers [37]. Considering the potential application on the vehicles, the pinch point temperature difference between the working fluid and PCM has been set at 10 °C. The evaporation temperature is defined as follows

$$T_{evap} = \begin{cases} T_{melt} - T_{e,pp}, & T_{melt} \le T_{PCM} \\ T_{PCM} - T_{e,pp}, & T_{melt} > T_{PCM} \end{cases} \tag{15}$$

The heat flux received from the evaporator and heat dissipation at the condenser

$$Q_{in} = m_{wf}\left(h_2 - h_3\right) \tag{16}$$

$$Q_{out} = Cp_c m_c \left(T_4 - T_1\right) \tag{17}$$

The work consumed by the pump can be calculated by the equations below

$$h_2 = h_1 + \left(h_{2s} - h_1\right)/\eta_{sP} \tag{18}$$

$$W_p = m_{wf}\left(h_2 - h_1\right) \tag{19}$$

For the expander

$$h_4 = \eta_{sE}\left(h_{4s} - h_3\right) + h_3 \tag{20}$$

$$W_e = m_{wf}\left(h_3 - h_4\right) \tag{21}$$

Then ORC net power and thermal efficiency

$$W_{net} = W_e - W_p \tag{22}$$

$$\eta_{th} = W_{net}/Q_{in} \tag{23}$$

The main parameters used in the calculation process are listed as Table 2. The isentropic efficiency for expander and pump are conservatively selected as reported by reference [37]. Considering the practical vehicle application conditions, the condensing temperature is set within the range of 35~60 ℃ [14, 24], in this paper it is set as 45 ℃. The heat transfer coefficients of working fluid in the liquid state, two-phase state and vapour state are given reference value [36]. The organic fluid enthalpies and other parameters are functions of the evaporating temperature chosen for the ORC and they are calculated with REFPROP. The above model is solved by MATLAB.

Table 2. Parameters used in the ORC calculations

Parameters	Value
The inlet temperature of the cooling water	25 ℃
Condensing temperature of working fluid T_1	45 ℃
Evaporator pinch point temperature difference $T_{e,pp}$	10 ℃
Expander isentropic efficiency η_{sE}	70%
Pump isentropic efficiency η_{sP}	80%
Heat transfer coefficient at liquid zone $h_{wf,l}$	260 $W \cdot m^{-2} K^{-1}$
Heat transfer coefficient at two-phase zones $h_{wf,tp}$	900 $W \cdot m^{-2} K^{-1}$

4. Results and discussion

The investigation of PCM options within the fluctuation range of the vehicle engine exhaust was studied on an ORC system integrated with single LTES for the purpose of selecting

potential PCM for the dynamic heat source. The performance of the ORC system with single LTES under different LTES volume has been evaluated based on the obtained proper PCM. Moreover, the performance of three different ORC-LTES systems including double LTES scheme and single LTES scheme were compared in a complete charging-discharging period under the dynamic heat source.

4.1 Analysis of PCM options under steady heat source conditions

The effects of PCM options under different steady heat sources were analysed. The selection of potential PCM is important and necessary under stead heat source conditions because the exhaust temperature of the vehicle engines fluctuates from 200 ℃ to 450℃. Considering the requirement of compactness for vehicle application, the volume of LTES is set as 50 L. In this study, three different conditions of steady heat source are set at T=250 ℃, 325 ℃ and 400 ℃, and the mass flow rate is set at m=0.2 kg/s. The duration of the charging process is set to be 60 minutes. Both the charging process and the discharging process were evaluated under several kinds of PCMs considering the relationship between the heat source temperature and the melting temperature in each case. Thermal losses are neglected and the initial condition of the store is set as the minimum temperature required to run the ORC system. The initial condition of the PCMs is assumed to be fully solidified and the internal energy increases isothermally as the melting of the PCM occurs. When the PCM is fully melted, the LTES stores heat sensibly and its temperature increases. Physical parameters of all the selected PCMs can be found in Table 1.

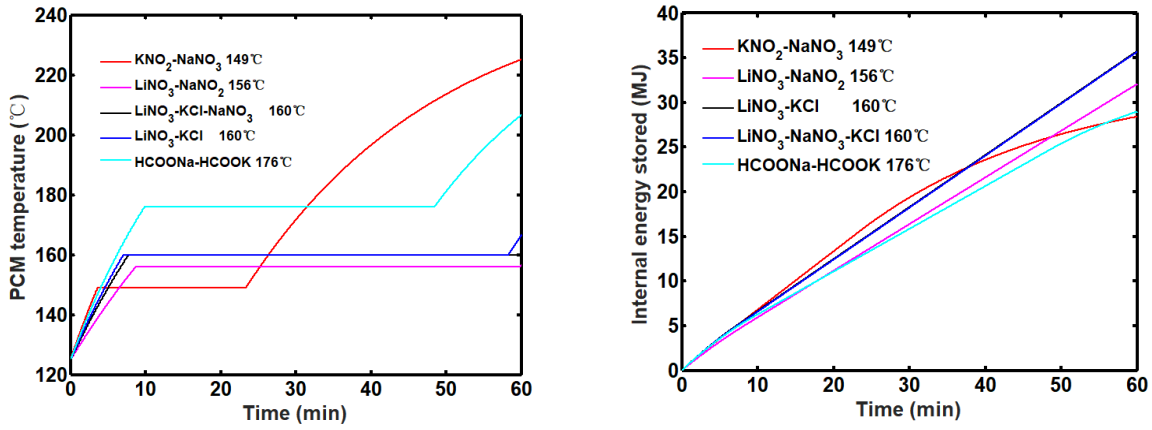

(a) PCM temperature evolution (b) Internal energy stored

Fig. 6. Performance of the LTES with different PCMs during the charging process (T=250 ℃)

1 Case 1: T=250 ℃, m=0.2 kg/s

2 The performance of the PCMs in the charging process has been illustrated in Fig. 6. Results
3 indicate within 60 minutes charging time, KNO_2-$NaNO_3$ and HCOONa-HCOOK have the
4 same maximum storage temperature (225 ℃) because of their small latent heat and specific
5 capacity while $LiNO_3$-$NaNO_2$ has the minimum storage temperature (156 ℃) due to its large
6 latent heat and specific capacity as shown in Fig. 6 (a). $LiNO_3$-KCl and $LiNO_3$-KCl-$NaNO_3$
7 have similar physical parameters with large latent heat， so they can store heat isothermally for
8 a longer period as shown in Fig. 6 (a), and they can keep a lower average temperature in the
9 charging process, which is beneficial for the heat transfer process. As indicated in Fig. 6 (b),
10 PCMs with larger latent heat can store more heat in the charging process. Compared to
11 KNO_2-$NaNO_3$ and HCOONa-HCOOK, $LiNO_3$-$NaNO_2$, $LiNO_3$-KCl and $LiNO_3$-KCl-$NaNO_3$
12 indicate lower maximum temperature and larger stored heat, which means these three PCMs

can maintain a steady LTES temperature for a longer time and have fewer heat losses in the charging process and is suitable for ORC system to working under the designed point.

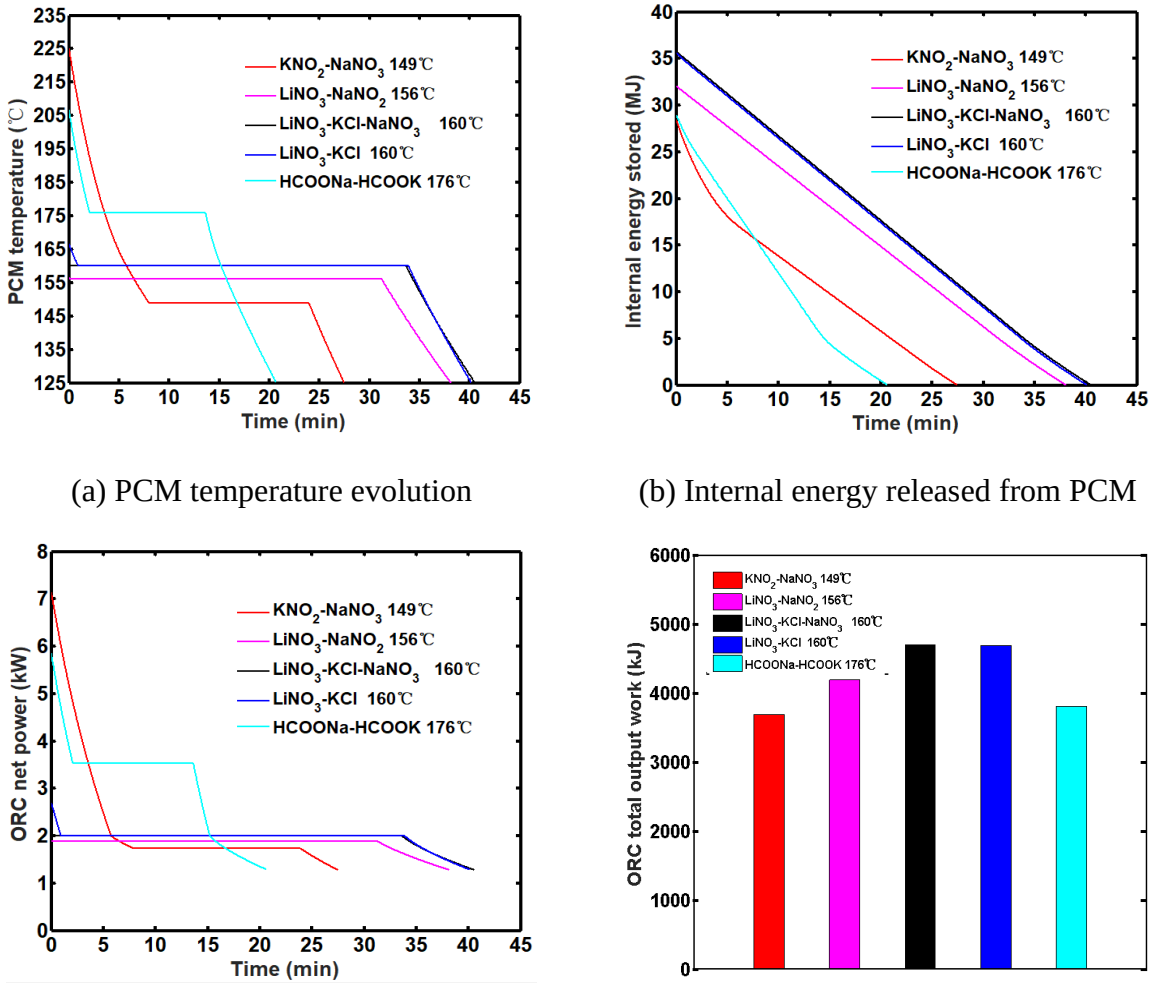

(a) PCM temperature evolution

(b) Internal energy released from PCM

(c) ORC power output

(d) ORC total power output

Fig. 7. Performance of the LTES with different PCMs in the discharging process (T=250 ℃)

Fig. 7 illustrates the performance of the PCMs in the discharging process. Results indicate the duration of discharging time for $LiNO_3$-KCl-$NaNO_3$ (41 min), $LiNO_3$-KCl (40.7 min) and $LiNO_3$-$NaNO_2$ (36 min) and are longer than that of KNO_2-$NaNO_3$ (27 min) and HCOONa-HCOOK (21 min). As shown in Fig. 7(c) it can be concluded that higher LTES temperatures would result in higher initial power outputs at the start of the ORC operation

period due to the increased evaporating temperature of ORC working fluid. The total-work output and the duration of the operating period are higher for the materials with the lower storage temperatures as the results plotted in Fig. 7 (d). Therefore, $LiNO_3$-KCl-$NaNO_3$ is the most suitable PCM among the five PCMs due to its longest duration of the operating period and largest total work output.

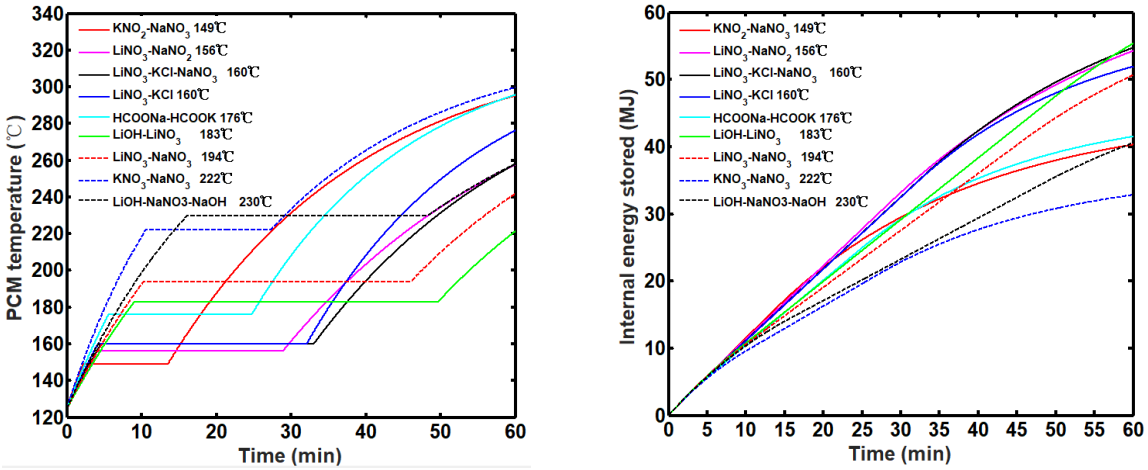

(a) PCM temperature evolution (b) Internal energy stored

Fig. 8. Performance of LTES with different PCMs in the charging process (T=325 ℃)

Case 2: T=325 ℃, m=0.2 kg/s

In order to find out proper materials for this case, PCMs studied in case 1 were also considered in this case and the PCMs with higher melting temperature were included. In Fig. 8, it can be found that the latent heat is the dominant factor that determines the duration of the discharging process and the final storage temperature among the selected PCMs. $NaNO_3$-KNO_3 shown the highest final storage temperature because of its smallest latent heat and it stored the minimal heat during the charging process. The final storage temperature of KNO_2-$NaNO_3$ and HCOONa-HCOOK were close to that of $NaNO_3$-KNO_3.

LiOH-$NaNO_3$-NaOH stores the second smallest heat because it maintains the relatively high average temperature in the charging process although it has the medium latent heat resulting in medium final storage temperature, which is not beneficial for the heat transfer between the PCM and the exhaust. The temperature evolution of $LiNO_3$-KCl is almost the same as that of $LiNO_3$-KCl-$NaNO_3$ before they completely melt due to the similar latent heat and specific heat capacity at solid state as shown in Fig. 8 (a). However, $LiNO_3$-KCl-$NaNO_3$ experiences a lower storage temperature and stores more heat than that of $LiNO_3$-KCl, because $LiNO_3$-KCl-$NaNO_3$ have a larger specific heat capacity at liquid state compared to $LiNO_3$-KCl. Results also indicate $LiNO_3$-$NaNO_2$ has a slightly smaller latent heat, but lager specific heat capacity compared with the above two PCMs. Therefore, it has approximately the same temperature evolution performance as $LiNO_3$-KCl and $LiNO_3$-KCl-$NaNO_3$. $NaNO_3$-$LiNO_3$ has almost equal latent heat but higher melting temperature to that of $LiNO_3$-KCl and $LiNO_3$-KCl-$NaNO_3$. It experiences lower final storage temperature and it stores less heat in the charging process. The storage temperature of LiOH-$LiNO_3$ is lowest among all the PCMs, but it stores the most heat during the charging process since it possesses the much larger latent heat than among the selected materials.

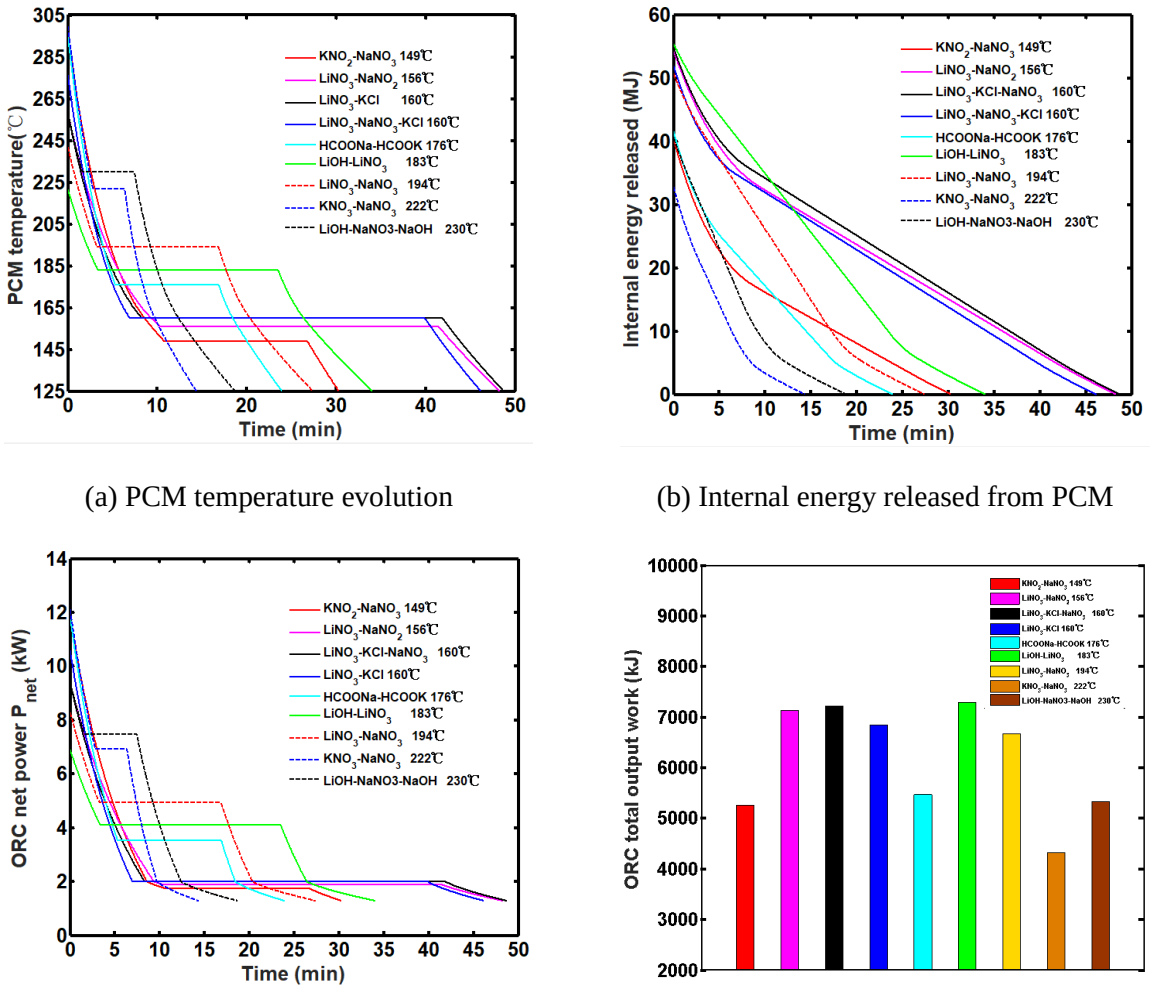

(a) PCM temperature evolution

(b) Internal energy released from PCM

(c) ORC power output

(d) ORC total power output

Fig. 9. Performance of the LTES with different PCM in the discharging process (*T*=325 ℃)

As shown in Fig. 9, $LiNO_3$-KCl-$NaNO_3$ (48.8 min) has the longest duration of the discharging process among all the candidates. PCMs such as $LiNO_3$-$NaNO_2$ (48.3 min), $LiNO_3$-KCl (46.2 min) and LiOH-$LiNO_3$ (34.1 min), who has large latent heat and low melting temperature, shown better performance on the ORC operating duration than that of other candidates. ORC evaporating temperature is determined by the PCM temperature and pinch point temperature difference in the discharging process. Therefore, lower ORC evaporating temperature can result in lower demand for PCM temperature and potentially

store more heat, which can maintain the ORC operation time to be longer. The performance of ORC power output has been shown in Fig. 9 (c). LiOH-$LiNO_3$ generates the maximum total power output among all the selected PCMs. $LiNO_3$-KCl-$NaNO_3$, $LiNO_3$-$NaNO_2$ and $LiNO_3$-KCl rank second, third and fourth, all of which are slightly smaller (1.1%, 2.3% and 6.1%, respectively) than LiOH-$LiNO_3$. The above three PCMs have longer ORC operating duration than LiOH-$LiNO_3$, which means they can stably deliver power for a long time for utilisation. Considering the ORC operating duration and total power output, $LiNO_3$-KCl-$NaNO_3$ is identified as the optimal candidate in this case study.

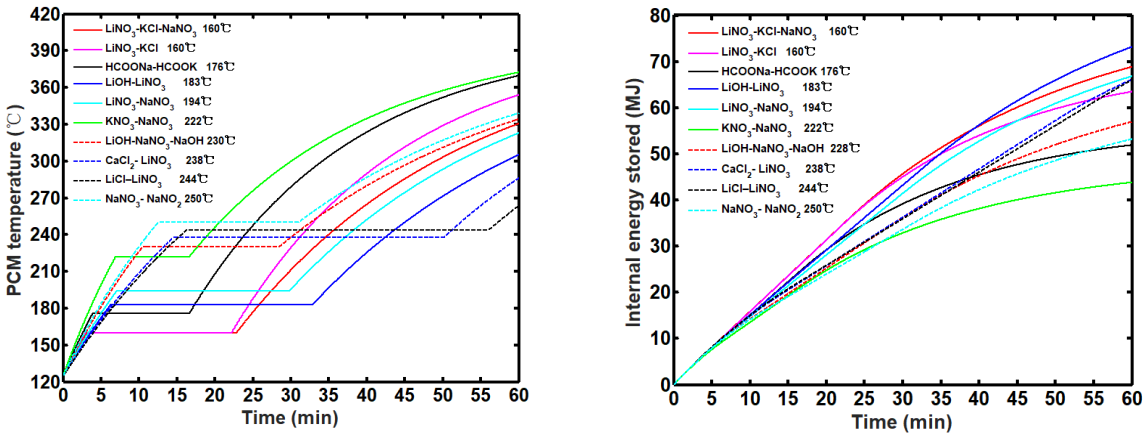

(a) PCM temperature evolution (b) Internal energy stored

Fig. 10. Performance of LTES with different PCM in the charging process (T=400 °C)

Case 3: T=400 °C, m=0.2 kg/s

In this case, PCMs with higher melting temperature were studied while PCMs with low melting temperature studied in case 2 were excluded because of the increase in exhaust temperature. As previously discussed in case 1 and 2, PCM that has large latent heat and low melting temperature experience lower final storage temperature and store more heat. PCMs

with large latent heat such as LiCl-$LiNO_3$ (263 ℃), $CaCl_2$-$LiNO_3$ (286 ℃), LiOH-$LiNO_3$ (305 ℃), $NaNO_3$-$LiNO_3$ (322 ℃) and $LiNO_3$-KCl-$NaNO_3$ (330 ℃) shown lower final storage temperature and store more heat than other PCMs in the charging process as illustrated in Fig. 10 (a) and (b). However, LiOH-$LiNO_3$ and $LiNO_3$-KCl-$NaNO_3$ shown better heat storage ability than that of LiCl-$LiNO_3$, $CaCl_2$-$LiNO_3$ and LiOH-$LiNO_3$. Results indicate other PCMs would lead to higher final storage temperature and store less heat since they have improper latent heat and melting temperature in the operational conditions of the case study.

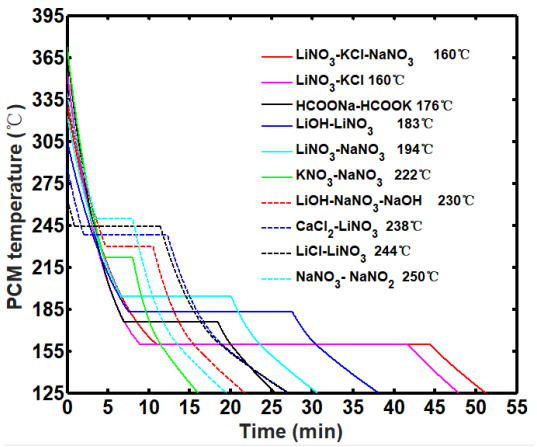

(a) PCM temperature evolution

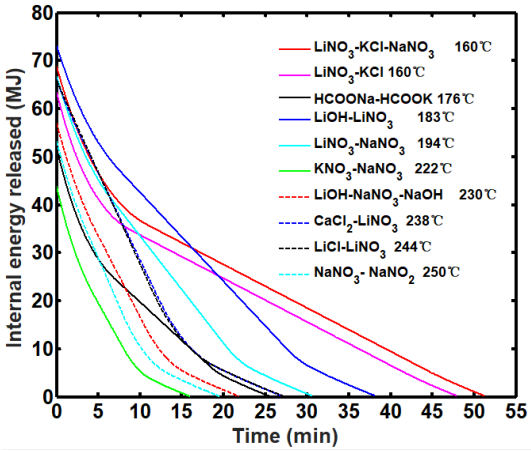

(b) Internal energy released from PCM

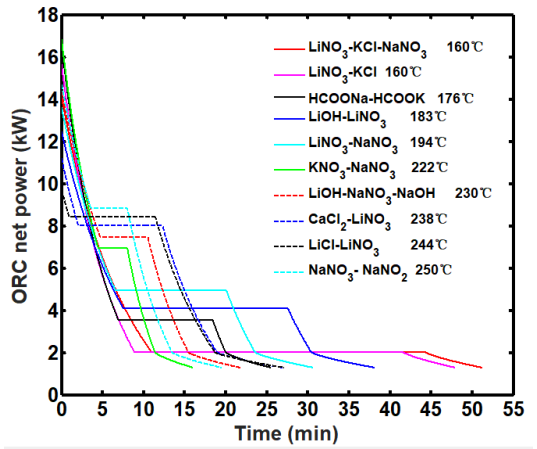

(c) ORC power output

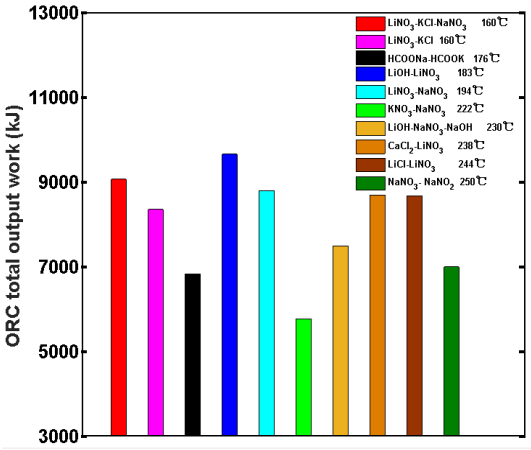

(d) ORC total power output

Fig. 11. Performance of the LTES with different PCM in the discharging process (T=400 ^{o}C)

Fig. 11 illustrated the performance of different PCM during the discharging process. ORC operating duration of $LiNO_3$-KCl-$NaNO_3$ (51.2 min), $LiNO_3$-KCl (47.9 min) and LiOH-$LiNO_3$ (38.1 min) are longer than other candidates. Although PCMs such as $CaCl_2$-$LiNO_3$ (26.9 min) and LiCl-$LiNO_3$ (27.1 min) possesses large latent heat, their melting temperature is quite high, leading to higher evaporating temperature and larger mass flow rate of ORC working fluid. Therefore, the stored heat can be discharged faster and the ORC working duration is shorter. Other PCMs with small latent heat including $NaNO_3$-KNO_3 (16.0 min), $NaNO_3$-NaOH (19.5 min) and LiOH-$NaNO_3$-NaOH (21.8 min) shows the shortest ORC working duration. In terms of the total ORC power output, LiOH-$LiNO_3$ delivers the largest total power output because of its largest latent heat and low melting temperature. The total power output of $LiNO_3$-KCl-$NaNO_3$ is slightly smaller (about 5.5%) than that of LiOH-$LiNO_3$. Compared to case 2, the difference in total power output between $LiNO_3$-KCl-$NaNO_3$ and LiOH-$LiNO_3$ is increased from 1.1% to 5.5%. However, the difference of total power output between $NaNO_3$-$LiNO_3$ and $LiNO_3$-KCl-$NaNO_3$ is decreased from 7.5% to 3.0%, which indicates that the most proper melting temperature of PCM increases with the improvement of heat source temperature. PCMs with lower melting temperature melt faster with the increase of heat source due to higher final storage temperature is shown in Fig. 8 (a) and Fig. 10 (a). For $LiNO_3$-KCl-$NaNO_3$ and $LiNO_3$-KCl, the difference of total power output between them is also enlarged compared to that of case 2, because $LiNO_3$-KCl-$NaNO_3$ has larger specific heat capacity in the liquid state. Considering

ORC operating duration and total power output as well as the temperature range of heat source conditions for engine exhaust heat recovery, $LiNO_3$-KCl-$NaNO_3$ is expected to have better comprehensive performance.

It can be summarised that PCM with large latent heat and low melting temperature can store a large amount of heat in the charging process and have low final storage temperature. Moreover, the PCMs held the stated characteristics can produce long ORC operating duration and large total power output. Under the three case study conditions, $LiNO_3$-KCl-$NaNO_3$ is proved to be the most suitable PCM among all the studied PCMs. $LiNO_3$-KCl-$NaNO_3$ delivers the highest total ORC output and has the longest ORC working duration in case 1. Although LiOH-$LiNO_3$ delivers the highest total power output both in case 2 and 3, its ORC working durations are only 34.1 min and 38.1 min. For $LiNO_3$-KCl-$NaNO_3$, the total ORC power output in case 2 and 3 is merely 1.1% and 5.5% smaller than that of LiOH-$LiNO_3$. $LiNO_3$-KCl-$NaNO_3$ has the longest ORC working duration for 48.8 min and 51.2 min in case 2 and 3, respectively. Therefore, the following section investigated the PCM-based ORC system under dynamic heat source conditions using $LiNO_3$-KCl-$NaNO_3$ as the phase change material.

4.2 System performance under dynamic heat source conditions

Based on this dynamic heat source shown in Fig. 5, the performance of ORC with LTES was simulated and analysed. The charging process and discharging process of LTES using $LiNO_3$-KCl-$NaNO_3$ under this dynamic heat source were investigated.

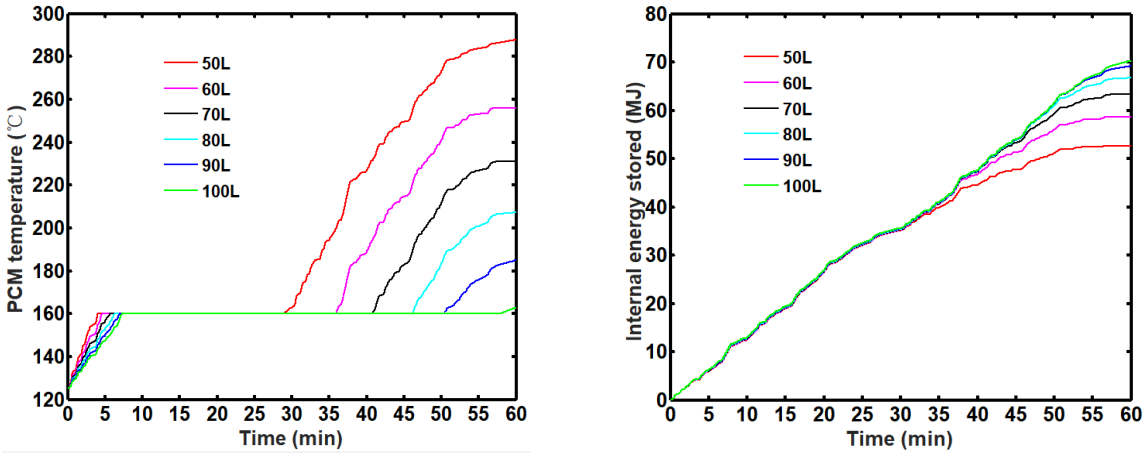

(a) PCM temperature evolution (b) Internal energy stored by PCM

Fig. 12. Temperature evolutions and internal energy stored by $LiNO_3$-KCl-$NaNO_3$ under different LTES volume

Fig. 12 shows the temperature evolution and internal energy stored by $LiNO_3$-KCl-$NaNO_3$ under different LTES volume. The larger LTES volume means the heavier weight of PCM and larger heat transfer area between the exhaust and PCM. As shown in Fig. 12(a), it can be found that the final heat storage temperature decreases with the increase of the LTES volume. The final storage temperature of LTES with a volume of 100L is 162.8 ℃ while it is 287.8 ℃ for LTES with a volume of 50 L. Due to the phase change process of PCM, the large fluctuation of engine exhaust can be significantly reduced, which is beneficial to the waste heat recovery using ORC. Meanwhile, the duration of constant temperature has a positive correlation to the LTES volume. When the duration of the melting process is longer, the duration of sensible heat storage process can be shorter. Furthermore, during sensible heat storage processes, the great fluctuation of the heat source is also reduced despite some little irregularity of temperature evolution. Results in Fig. 12 (b) indicate the total internal energy stored by LTES increases with the rise of the LTES volume but the increase rate is reduced. It

can, therefore, be concluded that the volume of LTES should be properly designed in order to obtain low final storage temperature and store a high amount of heat considering the requirement of the low cost of LTES devices and compactness.

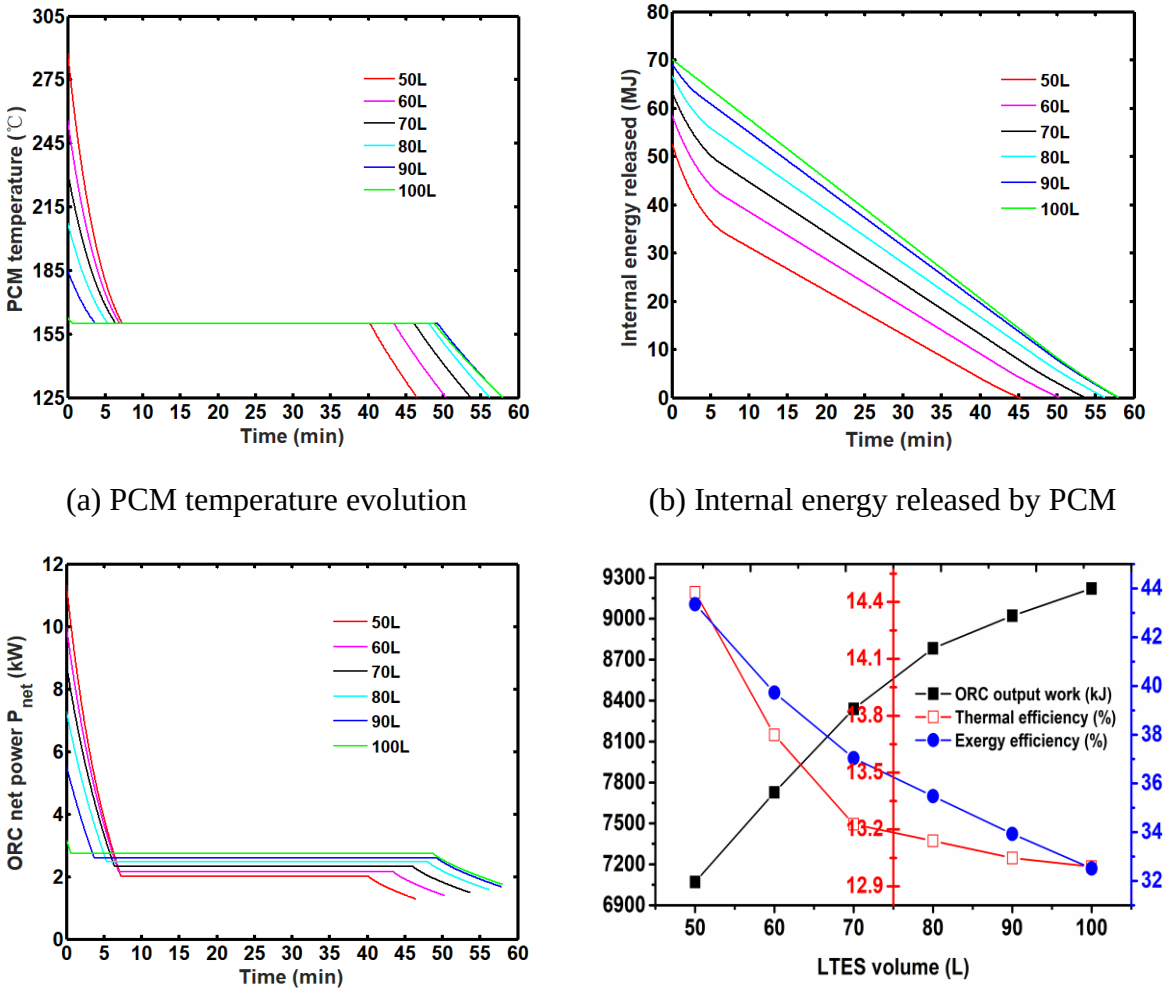

(a) PCM temperature evolution

(b) Internal energy released by PCM

(c) ORC power output P_{net}.

(d) Output work, thermal and exergy efficiency

Fig. 13. Performance of the LTES with $LiNO_3$-KCl-$NaNO_3$ under different LTES volume in the discharging process

Fig. 13 illustrates the performance of ORC under different LTES volumes during the discharging process. The temperature evolution in the discharging process shown in Fig. 13 (a) indicates that LTES maintains a constant temperature in most of the time because of the

solidification process under. Furthermore, the duration of constant temperature increases with the LTES volume without exceeding 90 L, but the increase rate of duration decreases as the LTES volume increase. The ORC system could work under steady state as a result of the relatively constant temperature of PCM, which is depicted in Fig. 13 (b) and (c). The net power of the ORC system under each condition first decreases in the sensible heat discharging process of liquid PCM, then it maintains constant during the solidification process of PCM. Once the solidification process is completed, it continues to decrease until the PCM temperature is close to the driving temperature of ORC in the sensible heat discharging process of solid PCM. ORC system can deliver the largest net power of 2.74 kW for about longest time of 48.2 min in the condition of 100 L while the value is 2.00 kW for about shortest time of 33.6 min in the condition of 50 L. The total output work of ORC, thermal efficiency and exergy efficiency in the whole discharging process are shown in Fig. 13 (d). It can be found that the total output work improves with the increase of LTES volume, which is because the total internal energy stored by LTES increases with the rise of the LTES volume, but the increase rate is reduced. The condition of 100 L LTES provides 30.4% larger total output work than that of 50 L LTES, while it is merely 1.5% larger than that of 90 L LTES. 50-L LTES corresponds the maximum thermal and exergy efficiency while the 100-L LTES leads to the minimum ones. The reason is due to the final storage temperature of LTES shown in Fig. 12(a). The higher LTES temperature during the ORC working process (discharging process) can lead to larger thermal efficiency and exergy efficiency because of higher evaporating temperature. In addition, the thermal efficiency and exergy efficiency both decrease with the increase of LTES volume.

4.3 Performance comparison of double and single LTES

The previous investigations and analysis are based on single LTES. However, single LTES could not absorb heat from the exhaust gas and release heat to ORC working fluid at the same time because heat fluxes between both sides are not balanced and the temperature of LTES

cannot be easily monitored and controlled. The proposed solution is to adopt double LTES, which can store excess thermal energy and releases it on demand. Three operating modes listed in Table 3 for single LTES and double LTES are designed to evaluate and compare the performances of different ORC systems. LTES in all the operating modes is assumed to be the solid state with an initial temperature of 125 ℃. The dynamic heat source is shown in Fig. 11 is assumed to be a periodic heat source with the period of 30 min in this section.

Table 3. Design and description of different modes for LTES

Modes	LTES Volume	LTES Number	Descriptions
Mode 1	50L (A)+50L (B)	Double	Discharging process of LTES A (B) starts when the PCM fully melts and charging process of LTES B (A) starts at the same time. The charging process for both A and B starts when the temperature of PCM decreases to 125 ℃. That is, the charging process and discharging process for LTES A and B operate alternatively.
Mode 2	50L	Single	Discharging process starts when the PCM fully melts and the charging process starts when the temperature of PCM decreases to 125 ℃.
Mode 3	100L	Single	Discharging process starts when the PCM fully melts and the charging process starts when the temperature of PCM decreases to 125 ℃.

Fig. 14 shows the performance of LTES and ORC system for three different modes in an integrated charging-discharging period. As for PCM temperature as shown in Fig. 14 (a), in mode 1, LTES A first enters the charging process and LTES B waits for the start of charging

process till the charging process of LTES A completes (Time elapsed from t_0 to t_1). Then LTES A starts its discharging process and ORC system starts recovering stored heat (from t_1 to t_3). LTES B starts its charging process at t_1 and ends at t_2 and from t_2 to t_3 it does not store heat. From t_3 to t_4 LTES A is during charging process while LTES B is during the discharging process. The whole process lasts for 107.3 min and ORC system works from t_1 to t_5 for 78.6 min. In mode 2, the charging process of LTES ends at t_6 and the discharging process finishes at t_7 (68.1 min). Considering the period of mode 2 is shorter than that of mode 1, LTES in mode 2 is assumed to continue experiencing an integrated charging process from t_7 to t_8 (97.7 min). The working duration of the ORC system is about 39.3 min. In mode 3, the charging process and discharging process last from t_0 to t_{10} (117.4 min), while the ORC system recovers waste heat for 59.9 min. The ORC working duration of mode 1 is significantly higher than that of mode 2 and 3, which means ORC system in mode 1 can deliver effective work for a longer period and can be easier to meet the demand of users.

In terms of the internal energy stored by LTES as shown in Fig. 14 (b), the energy stored by LTES A and B in mode 1 first increases and then it decreases due to the switch between LTES A and B for charging and discharging process. The total internal energy stored by LTES A and B is relatively uniform and keeps above 35 MJ after the first charging process, which means the ORC system can be steadily operated within the designed conditions. In mode 2 the evolution of energy stored by LTES is the same as that of LTES A in mode 1, which changes with elapsed time periodically leading to the intermittent operation of the ORC system. The evolution of energy stored by LTES in mode 3 is similar to that of mode 2.

The results of ORC net power output are shown in Fig. 14 (c). In mode 1, the ORC system delivers an average net power of 2.0 kW for 78.6 min. In mode 3, ORC system delivers an average net power of 2.7 kW for 59.9 min due to the LTES volume of mode 3 is larger than that of mode 1, which leads to larger heat transfer area and more energy stored. In mode 2, ORC net power output is the same as that of LTES A in mode 1. As the period of mode 2 is shorter than that of mode 1, ORC net power output can last for a longer duration after t8, but ORC working duration is still shorter than that of mode 1. Fig. 14 (d) shows the ORC total output work in an integrated period for three different modes. In mode 1, the power output increase after the first discharging process and reaches 9.125 MJ during a period of 107.3 min. The ORC output work in mode 2 is about 4.557 MJ. In mode 3, the total ORC output work can attain 9.123 MJ at 117.4 min, which is slightly lower than that of mode 1 at 9.125 MJ. However, within the designed period t11, the ORC total power output of mode 1 is 17.2% higher than that of mode 3.

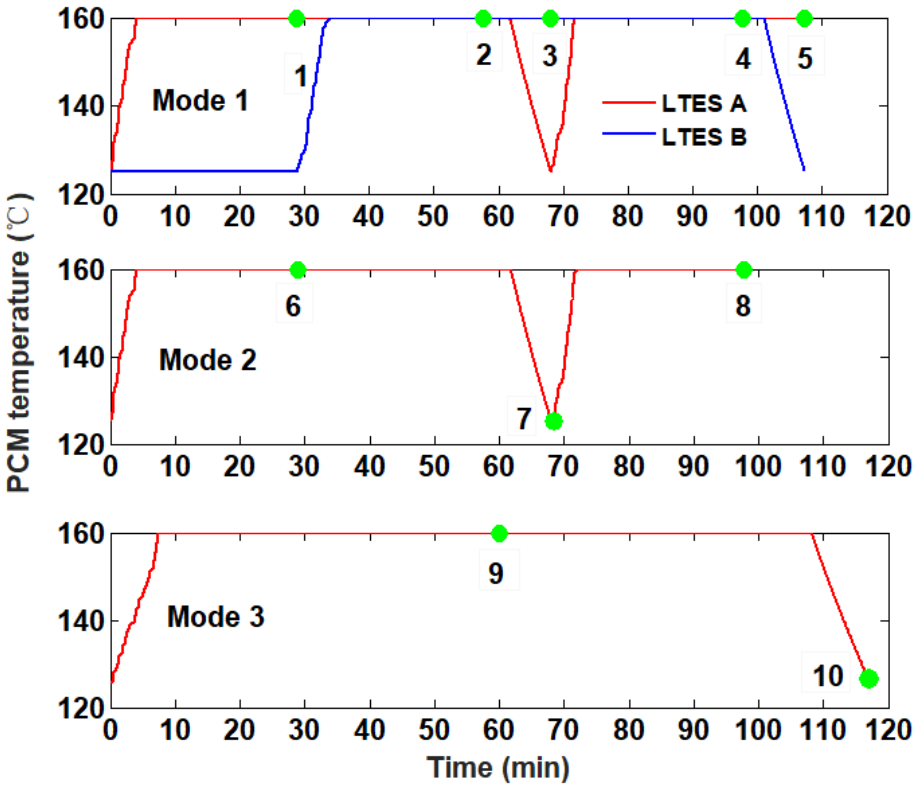

(a) Temperature evolution of LTES for three different modes

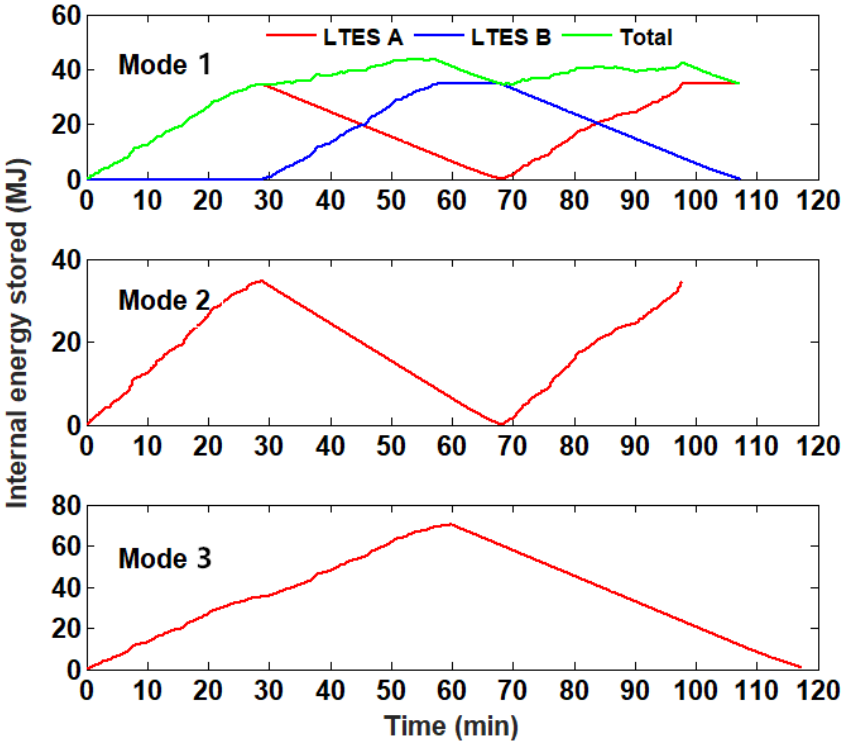

(b) Internal energy evolution of LTES for three different modes

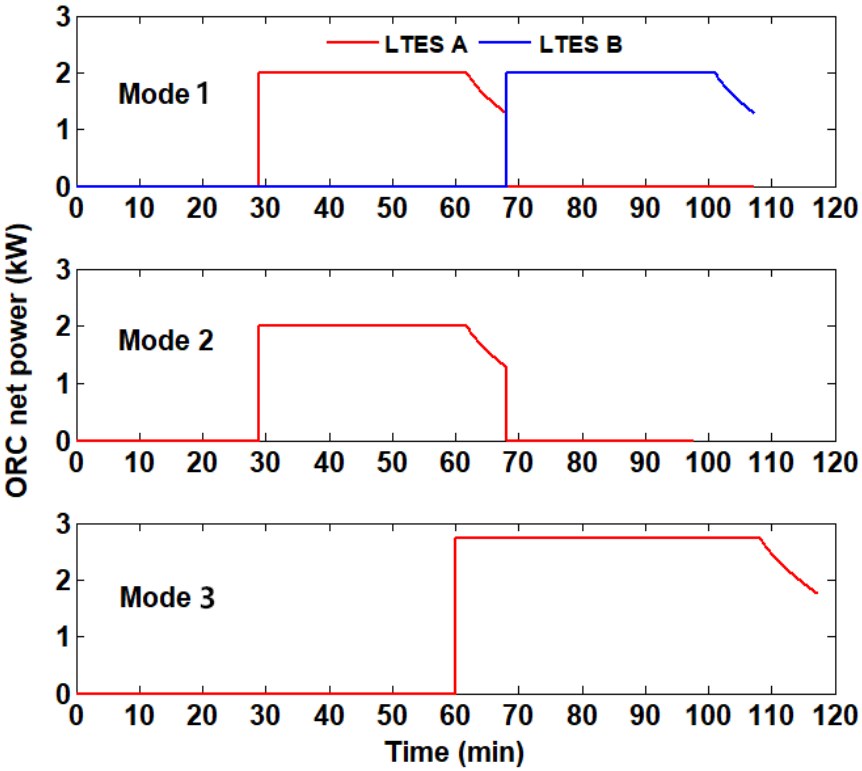

(c) ORC net power output with time for three different modes

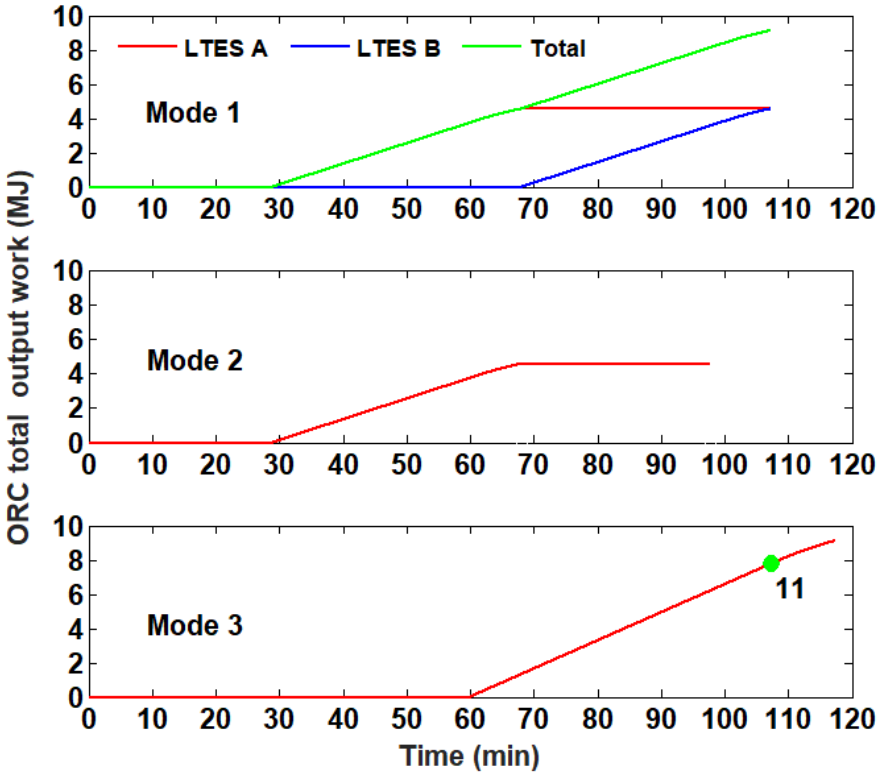

(d) Total ORC output work with time for three different modes

Fig. 14. Performances of LTES and ORC system for three different modes

4.4 Discussion on practical differences and costs

This section provides a short discussion about the practical differences and costs among the three different operating modes studied in section 4.3. For each mode, the size and investment for ORC are almost the same. For mode 1 and 2, the main difference between them is the amount of LTES tanks. The initial research and development of a 50-L LTES tank for mode 1 and mode 2 is the same, but the total initial investment for the whole system of mode 1 is larger than that of mode 2 since an additional LTES tank and auxiliary pipes are needed. Considering the much larger ORC total output work and working duration over a charging-discharging period, mode 1 is recommended because of its shorter payback time. As for mode 1 and mode 3, the LTES tank volume of mode 1 (50 L) is smaller than that of mode 3 (100 L), leading to a lower initial expenditure during the research and development process. Although the total LTES volume is equal to the that of mode 3, the whole initial investment for mode 1 is also lower than that of mode 3, because the scientific research and development expenditure for a new product is much higher than its commercialized price. In addition, the total output work of ORC for mode 1 is 9.125 MJ during a period of 107.3 min while it is 9.123 MJ for mode 3 during a period of 117.4 min, the corresponding ORC working durations for mode 1 and mode 3 are 78.6 min and 59.3 min, respectively. Therefore, mode 1 is more potential for engine waste heat recovery than mode 3. In conclusion, mode 1 possesses comprehensively larger total ORC output work and longer working duration than those of mode 2 and 3. Therefore, mode 1 is recommended among the three operating modes.

5. Conclusions

This paper investigated the potential application of PCM-based ORC system in order to overcome the fluctuation of the vehicle engine heat source. Performance of ORC system integrated LTES were evaluated under steady and dynamic heat source conditions. The investigation of the ORC system under different LTES volume and ORC-LTES modes were studied. This research has effectively supplemented the knowledge about the potential application of ORC system integrated with double LTES for engine waste heat recovery. Key findings could be drawn as follows,

(1) PCMs with large latent heat and low melting temperature indicated a lower final storage temperature and store more heat in the charging process. During the discharging process, the PCMs held the stated characteristic could have longer ORC operating duration and larger total output work. Results indicated among the selected PCM candidates, LiNO3-KCl-NaNO3 is the optimal thermal energy storage material considering its longest ORC operating duration and almost the largest ORC total output work.

(2) Results under dynamic heat source showed that the large fluctuation of engine heat source can be significantly reduced due to the phase change process of PCM. ORC net power and duration of delivering constant net power increase with the increase of LTES volume. 100 L LTES can improve the ORC total output work by 30.4% than that of 50 L. However, ORC output from 100 L LTES is only 1.5% higher than that of

90 L, which means optimal design methods should be adopted under targeted dynamic heat source conditions.

(3) Mode 1 (double LTES, 50 L+50 L) has the best comprehensive performance while Mode 2 (single LTES, 50 L) is the worst. The proposed double LTES (Mode 1) solution can steadily generate power from the ORC system and the Mode 1 can store the internal energy more uniform than that of Mode 2 and 3. The solution can effectively overcome the intermittent problem of single LTES system. The power output from ORC in Mode 1 delivers an average net power of 2.0 kW for 78.6 min in a period of 107.3 min while in Mode 3 it is 2.7 kW for 59.9 min in a period of 117.4 min. At the end of 2 hours operational time, the ORC total output work from Mode 3 can achieve 9.125 MJ, which is slightly higher than that of Mode 1 at 9.123 MJ. However, when the time is set at the designed condition for Mode 1, the ORC total output work of Mode 1 is 17.2% larger than that of Mode 3.

6. Suggestion for the future work

The proposed organic Rankine cycle integrating with double latent thermal energy storage (LTES) is a potential solution to overcome the fluctuation and intermittence of engine exhaust energy. In this work, the effects of different PCMs and LTES volume are preliminarily investigated to demonstrate the feasibility of the proposed system. In addition to the stated parameters, other important technical parameters include: (1) the design and optimisation of highly efficient thermal energy storage heat exchanger to meet the requirements of

compactness for transport application. This involves designing a compact latent thermal energy storage, achieving a perfect combination with heat exchanger and phase change materials. Relatively high energy storage density and heat transfer rate (charging-discharging rate) are the main technical barriers. (2) Operating and control strategy of the system is also a crucial factor to adapt to the variation of heat source and energy demand under different driving conditions, realising the high energy utilisation efficiency of the whole system. The characteristics of the engine exhaust gas are much distinguishing under different driving conditions (urban and suburban conditions). Therefore, PCM selection, ORC working fluid selection and switch strategy of double LTES should be further optimised according to the objective driving conditions.

Acknowledgement

The finical support from UK-China Joint Research and Innovation Partnership fund under the grant number 201703780098 and the grants from the National Natural Science Foundation of China under grant number No. 51806189 and No. 51476143. The authors also would like to thank the supports from NSFC-RS Joint Project under the grant number No. 5151101443 and IE/151256, from EPSRC through (EP/P001173/1) - Centre for Energy Systems Integration. The support from Cao Guang Biao High Tech Talent Fund, Zhejiang University are also highly acknowledged.

Reference

[1] Sadeghi M, Nemati A, ghavimi A, Yari M. Thermodynamic analysis and multi-objective optimization of various ORC (organic Rankine cycle) configurations using zeotropic mixtures. Energy. 2016;109:791-802.

[2] Chen L, Zhang Z, Lu Y, Zhang C, Zhang X, Zhang C, et al. Experimental study of the gaseous and particulate matter emissions from a gas turbine combustor burning butyl butyrate and ethanol blends. Applied Energy. 2017;195:693-701.

[3] Lu Y, Roskilly AP, Yu X. The Development and Application of Organic Rankine Cycle for Vehicle Waste Heat Recovery. Organic Rankine Cycle Technology for Heat Recovery: IntechOpen; 2018.

[4] Lu Y, Roskilly AP, Jiang L, Chen L, Yu X. Analysis of a 1 kW organic Rankine cycle using a scroll expander for engine coolant and exhaust heat recovery. Frontiers in Energy. 2017;11(4):527-34.

[5] Yu G, Shu G, Tian H, Wei H, Liu L. Simulation and thermodynamic analysis of a bottoming Organic Rankine Cycle (ORC) of diesel engine (DE). Energy. 2013;51:281-90.

[6] Zamfirescu C, Dincer I. Thermodynamic analysis of a novel ammonia–water trilateral Rankine cycle. Thermochimica Acta. 2008;477(1-2):7-15.

[7] Chen Y, Guo Z, Wu J, Zhang Z, Hua J. Energy and exergy analysis of integrated system of ammonia–water Kalina–Rankine cycle. Energy. 2015;90:2028-37.

[8] He W, Wang S, Lu C, Zhang X, Li Y. Influence of different cooling methods on thermoelectric performance of an engine exhaust gas waste heat recovery system. Applied Energy. 2016;162:1251-8.

[9] He W, Wang S, Zhang X, Li Y, Lu C. Optimization design method of thermoelectric generator based on exhaust gas parameters for recovery of engine waste heat. Energy. 2015;91:1-9.

[10] Lu Y, Roskilly AP, Tang K, Wang Y, Jiang L, Yuan Y, et al. Investigation and performance study of a dual-source chemisorption power generation cycle using scroll expander. Applied Energy. 2017;204:979-93.

[11] Lu Y, Wang Y, Dong C, Wang L, Roskilly AP. Design and assessment on a novel integrated system for power and refrigeration using waste heat from diesel engine. Applied Thermal Engineering. 2015;91:591-9.

[12] Bianchi M, De Pascale A. Bottoming cycles for electric energy generation: Parametric investigation of available and innovative solutions for the exploitation of low and medium temperature heat sources. Applied Energy. 2011;88(5):1500-9.

[13] Wang ZQ, Zhou NJ, Guo J, Wang XY. Fluid selection and parametric optimization of organic Rankine cycle using low temperature waste heat. Energy. 2012;40(1):107-15.

[14] Shu G, Li X, Tian H, Liang X, Wei H, Wang X. Alkanes as working fluids for high-temperature exhaust heat recovery of diesel engine using organic Rankine cycle. Applied Energy. 2014;119:204-17.

[15] Yang F, Cho H, Zhang H, Zhang J. Thermoeconomic multi-objective optimization of a dual

loop organic Rankine cycle (ORC) for CNG engine waste heat recovery. Applied Energy. 2017;205:1100-18.

[16] Liu H, Zhang H, Yang F, Hou X, Yu F, Song S. Multi-objective optimization of fin-and-tube evaporator for a diesel engine-organic Rankine cycle (ORC) combined system using particle swarm optimization algorithm. Energy Conversion and Management. 2017;151:147-57.

[17] Al Jubori AM, Al-Dadah R, Mahmoud S. New performance maps for selecting suitable small-scale turbine configuration for low-power organic Rankine cycle applications. Journal of Cleaner Production. 2017;161:931-46.

[18] Song J, Gu C-w. Performance analysis of a dual-loop organic Rankine cycle (ORC) system with wet steam expansion for engine waste heat recovery. Applied Energy. 2015;156:280-9.

[19] Song J, Gu C-w. Parametric analysis of a dual loop Organic Rankine Cycle (ORC) system for engine waste heat recovery. Energy Conversion and Management. 2015;105:995-1005.

[20] Yari M, Mehr AS, Zare V, Mahmoudi SMS, Rosen MA. Exergoeconomic comparison of TLC (trilateral Rankine cycle), ORC (organic Rankine cycle) and Kalina cycle using a low grade heat source. Energy. 2015;83:712-22.

[21] Yu X, Li Z, Lu Y, Huang R, Roskilly A. Investigation of an Innovative Cascade Cycle Combining a Trilateral Cycle and an Organic Rankine Cycle (TLC-ORC) for Industry or Transport Application. 2018;11(11):3032.

[22] Lai NA, Wendland M, Fischer J. Working fluids for high-temperature organic Rankine cycles. Energy. 2011;36(1):199-211.

[23] Shu G, Zhao M, Tian H, Wei H, Liang X, Huo Y, et al. Experimental investigation on thermal OS/ORC (Oil Storage/Organic Rankine Cycle) system for waste heat recovery from diesel engine. Energy. 2016;107:693-706.

[24] Shu G, Liu L, Tian H, Wei H, Yu G. Parametric and working fluid analysis of a dual-loop organic Rankine cycle (DORC) used in engine waste heat recovery. Applied Energy. 2014;113:1188-98.

[25] Katsanos CO, Hountalas DT, Pariotis EG. Thermodynamic analysis of a Rankine cycle applied on a diesel truck engine using steam and organic medium. Energy Conversion and Management. 2012;60:68-76.

[26] Alva G, Lin Y, Fang G. An overview of thermal energy storage systems. Energy. 2018;144:341-78.

[27] Miró L, Gasia J, Cabeza LF. Thermal energy storage (TES) for industrial waste heat (IWH) recovery: A review. Applied Energy. 2016;179:284-301.

[28] Dal Magro F, Jimenez-Arreola M, Romagnoli A. Improving energy recovery efficiency by retrofitting a PCM-based technology to an ORC system operating under thermal power fluctuations. Applied Energy. 2017;208:972-85.

[29] Dal Magro F, Savino S, Meneghetti A, Nardin G. Coupling waste heat extraction by phase change materials with superheated steam generation in the steel industry. Energy. 2017;137:1107-18.

[30] Freeman J, Guarracino I, Kalogirou SA, Markides CN. A small-scale solar organic Rankine cycle combined heat and power system with integrated thermal energy storage. Applied Thermal Engineering. 2017;127:1543-54.

[31] Manfrida G, Secchi R, Stańczyk K. Modelling and simulation of phase change material latent heat storages applied to a solar-powered Organic Rankine Cycle. Applied Energy. 2016;179:378-88.

[32] Wang XD, Zhao L, Wang JL, Zhang WZ, Zhao XZ, Wu W. Performance evaluation of a low-temperature solar Rankine cycle system utilizing R245fa. Solar Energy. 2010;84(3):353-64.

[33] Pereira da Cunha J, Eames P. Thermal energy storage for low and medium temperature applications using phase change materials – A review. Applied Energy. 2016;177:227-38.

[34] Nardin G, Meneghetti A, Dal Magro F, Benedetti N. PCM-based energy recovery from electric arc furnaces. Applied Energy. 2014;136:947-55.

[35] Tao C, Lei Z, Weilin Z, Zhang Y. heat storage ORC system for vehicle ICE exhaust heat recovery. 3rd International Seminar on ORC Power Systems, October 12-14, 2015, Brussels, Belgium. 2015.

[36] Li S, Ma H, Li W. Dynamic performance analysis of solar organic Rankine cycle with thermal energy storage. Applied Thermal Engineering. 2018;129:155-64.

[37] Vaja I, Gambarotta A. Internal Combustion Engine (ICE) bottoming with Organic Rankine Cycles (ORCs). Energy. 2010;35(2):1084-93.